Contents lists available at ScienceDirect

Palaeogeography, Palaeoclimatology, Palaeoecology

Invited Research Article

Low oxygen isotope values of fossil cellulose indicate an intense monsoon in East Asia during the late Oligocene

Junbo Ren [a,b], Brian A. Schubert [b,*], William E. Lukens [c], Cheng Quan [d]

[a] College of Earth Sciences, Jilin University, Changchun 130061, China
[b] School of Geosciences, University of Louisiana at Lafayette, Lafayette, LA 70504, USA
[c] Department of Geology and Environmental Science, James Madison University, Harrisonburg, VA 22807, USA
[d] School of Earth Science and Resources, Chang'an University, Xi'an 710054, China

ARTICLE INFO

ABSTRACT

The late Oligocene is an important deep-time analog for understanding future changes in the strength of the East Asian monsoon: it represents a climate warmer than today, yet follows the nascent uplift of the Tibetan–Himalayan orogeny during the Eocene Epoch. Here we quantify monsoon strength based on new oxygen isotope measurements on cellulose ($\delta^{18}O_{cell}$) extracted from modern and fossil wood from southern China. Tree-ring $\delta^{18}O_{cell}$ values have previously been used to track Holocene climate variations in East Asia, as $\delta^{18}O_{cell}$ values are primarily controlled by meteoric water $\delta^{18}O$ ($\delta^{18}O_{MW}$) and relative humidity. We find the $\delta^{18}O_{cell}$ values measured on the modern samples (25.7 to 29.1‰ VSMOW) are consistent with other $\delta^{18}O_{cell}$ records from trees growing in southern China under the present-day monsoon climate. However, fossil wood $\delta^{18}O_{cell}$ values (21.0 to 24.1‰ VSMOW) are significantly lower than those from living trees in the region, and instead overlap with values from modern high latitudes and high elevations. We show that these low $\delta^{18}O_{cell}$ values are best explained by much higher rainfall amounts in southern China during the late Oligocene, with monthly wet-season rainfall that may have been ~60% greater than today based on modern relationships. These data represent the first seasonal rainfall estimates for southern China during the late Oligocene and signify an intensification of the region's current monsoonal rainfall patterns. We speculate that significantly greater monsoon rainfall is therefore possible in the region under a warmer climate.

1. Introduction

Strong seasonality in precipitation, with wet summers and dry winters, characterizes the monsoon climate across East Asia today. Models indicate that monsoon intensity, measured as the amount of summer rainfall, may increase with global warming (Takahashi et al., 2020), but projected changes have large uncertainties and substantial intermodel variability (Chevuturi et al., 2018), and the role of anthropogenic activity (i.e., aerosol emission) on monsoon strength is still highly debated (Bollasina et al., 2011; Dong et al., 2019; Kim et al., 2016; Mu and Wang, 2021). Paleoclimate records from intervals of warmer global climate may therefore be informative for understanding monsoon dynamics in a warmer world. Analysis of paleo-monsoon strength is commonly inferred from oxygen isotope measurements of speleothems (Cheng et al., 2016; Cosford et al., 2008; Liu et al., 2020), but these records are limited to the Quaternary, when CO_2 levels were lower than today. Studies of

monsoon strength in deep time (pre-Quaternary) indicate a strong link between CO_2 and rainfall dating back to the Eocene (Licht et al., 2014), while others highlight the important role of paleogeography on monsoon intensity (Farnsworth et al., 2019). Although the mechanism is debated, recent work provided firm evidence for an East Asian Monsoon-style system, with wet summers relative to winters, prior to the Neogene (Vornlocher et al., 2021), but quantitave estimates of the amount of wet-season rainfall in the late Oligocene are lacking. Here we provide new measurements of the oxygen isotope value of cellulose ($\delta^{18}O_{cell}$) extracted from modern and late Oligocene fossil wood in order to determine how monsoon rainfall during the late Oligocene compares to today. The late Oligocene is an ideal period to study the effect of global temperature on monsoon intensity because it represents the likely trajectory for Earth's climate system as CO_2 emissions continue to rise unabated (Westerhold et al., 2020). It also represents a critical period in central Tibetan uplift (Fang et al., 2020; Su et al., 2019), and therefore is

---

* Corresponding author.
E-mail addresses: junbo.ren@louisiana.edu (J. Ren), schubert@louisiana.edu (B.A. Schubert), lukenswe@jmu.edu (W.E. Lukens), quan@chd.edu.cn (C. Quan).

an essential yet understudied interval of time for investigating Asian monsoon dynamics in deep-time.

Determination of $\delta^{18}O_{cell}$ value from living trees has long been used to quantify recent climate change (Brienen et al., 2012; Knorre et al., 2010; Loader et al., 2010; Loader et al., 2007; McCarroll and Loader, 2004; Poussart et al., 2004; Rinne et al., 2013; Saurer et al., 2008; Treydte et al., 2006; Young et al., 2015), including in monsoon regions of East Asia (e.g., Sakashita et al., 2016; Xu et al., 2016). Application of these techniques to well-preserved fossil wood collected from pre-Quaternary sediments has allowed for new quantitative climate data in deep time (Jahren and Sternberg, 2002, 2003, 2008; Richter et al., 2008a; Wolfe et al., 2012). These studies all rely on empirical relationships between the stable oxygen isotope composition of tree-ring cellulose ($\delta^{18}O_{cell}$) and that of meteoric water ($\delta^{18}O_{MW}$) (Csank et al., 2013; Olson et al., 2020; Richter et al., 2008b; Saurer et al., 2016; Sternberg et al., 2007; Waterhouse et al., 2002), which can then be related to precipitation or temperature depending on the environment in which the plant grew: $\delta^{18}O_{MW}$ values in low-latitude sites respond more to rainfall amount (Araguás-Araguás et al., 1998; Brienen et al., 2012; Dayem et al., 2010; Gonfiantini et al., 2001; Xie et al., 2011), while $\delta^{18}O_{MW}$ values in middle to high-latitude sites are affected more by changes in temperature (Bowen, 2008; Dansgaard, 1964; Schubert and Jahren, 2015). We leverage these earlier works to present the first estimates for wet-season rainfall in southern China during the late Oligocene based on the $\delta^{18}O_{cell}$ value of well-preserved wood fossils, thus providing data on seasonal rainfall intensity in this monsoon region under a warmer climate state.

2. Materials and methods

Mummified fossil wood samples were collected from the upper Yongning Formation near Nanning in the Guangxi Zhuang Autonomous Region of South China (22°52′50" N, 108°25′2″ E; elevation = ~80 m; Fig. 1) (Quan et al., 2016). The upper Yongning Formation is a lacustrine deposit dated to the late Oligocene based on palynology and mammalian

fossils (Quan et al., 2016). For this study, we selected 64 mummified wood samples representing the genus *Castanopsis* (Huang et al., 2018) for cellulose extraction and oxygen isotope analysis. This genus is considered an important paleoecological indicator of subtropical evergreen forests (Gee et al., 2003), and are currently restricted to regions of east and southeast Asia (Huang et al., 2018). Living *Castanopsis* trees growing in the region have maximum rooting concentrations within the upper 0.3 m of the soil (Hao et al., 2006). Such shallow rooted trees may better record annual variations in $\delta^{18}O_{MW}$ (McCarroll and Loader, 2004; Waterhouse et al., 2002) than more deeply rooted species or trees growing in drier climates (e.g., Huang et al., 2019a; Huang et al., 2019b).

Radial cores (QXS21A and QXS24A, Fig. 1) were also collected from two living *Pinus massoniana* trees growing at nearby Qingxiushan Hill, Nanning (22°47′23.35" N, 108°23′4.26″ E, elevation = 223 m). The site has a humid, monsoon climate, with 63% of the total annual rainfall falling in only four months (May through August) (Fig. 2). Annual growth rings (entire earlywood and latewood) were sampled by hand using a razor blade across the years 1990–2000 to produce an annually resolved $\delta^{18}O_{cell}$ record. This period was chosen because it: 1) represented a wide range of wet-season (May through August) rainfall (482 to 1267 mm), and 2) avoided potential juvenile effects on $\delta^{18}O_{cell}$ value in the early portion of the trees' growth (Büntgen et al., 2020; Duffy et al., 2019). A total of 22 annual growth rings (11 per tree) were collected for stable isotope analysis.

We extracted α–cellulose from bulk samples of the fossil wood and individual tree rings of the modern wood following a method modified from Brendel et al. (2000). Because of the low cellulose yields in the fossil wood relative to the modern wood, we increased the amount of fossil wood starting material and proportionally adjusted the volume of reagent used. Lignin was removed by nitric acid and acetic acid, and lipids were removed by ethanol and acetone, and then treated with 17% sodium hydroxide solution to obtain α–cellulose. Dry α–cellulose samples were then weighed into silver capsules, and $\delta^{18}O_{cell}$ values were determined using a High–Temperature–Conversion Elemental Analyzer
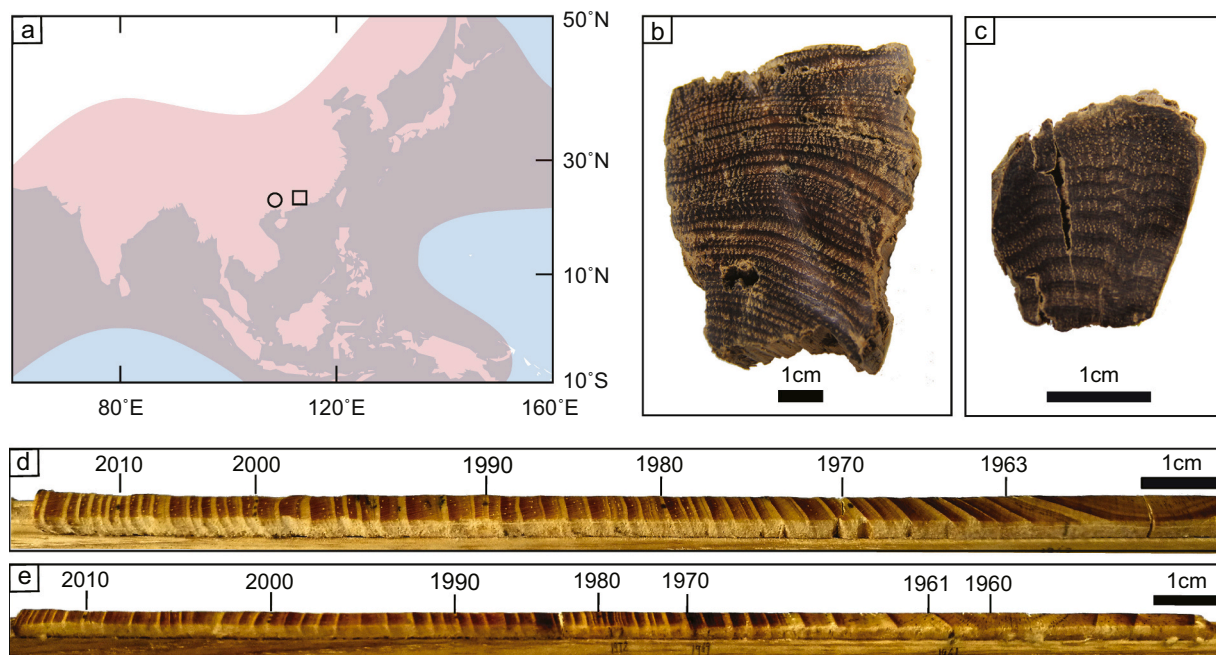

Fig. 1. a) Location of Nanning, China (circle) and Guangzhou, China (square) within the present-day monsoon region (pink: as reported within (Ramage, 1971) and (Wang and Ding, 2008)). Note this area includes the East Asia summer monsoon, western North Pacific summer monsoon, and Indian summer monsoon (Wang and LinHo, 2002). All of these locations experience high rainfall seasonality today. b-c) Photographs of mummified fossil wood samples: b) NNW015 and c) NNW037, respectively. d-e) Photographs of the two modern cores: d) QXS21A and e) QXS24A. (For interpretation of the references to colour in this figure legend, the reader is referred to the web version of this article.)
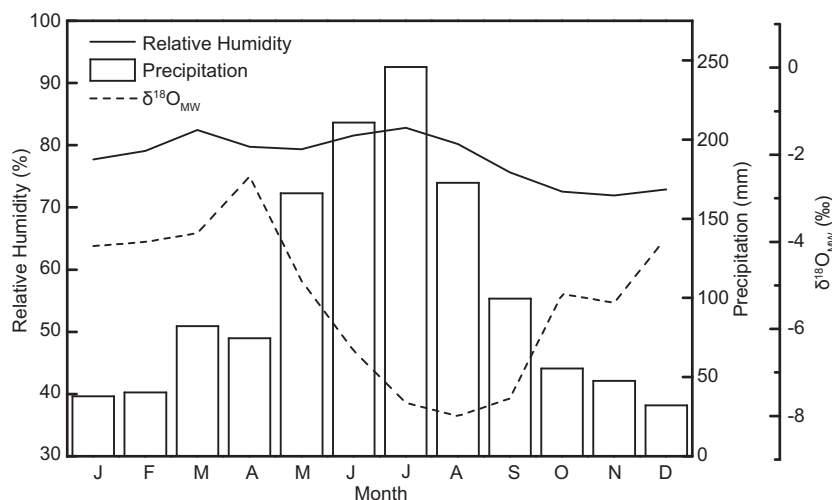
Fig. 2. Monthly average relative humidity, precipitation, and $\delta^{18}O_{MW}$ value for Nanning, China. Note that the lowest $\delta^{18}O_{MW}$ values occur in summer when precipitation is greatest. Climate data are from the China Meteorological Data Service Center (2018) for our study period (1990–2000); $\delta^{18}O_{MW}$ data are from Bowen et al. (2005).

coupled with a Delta–V Advantage Mass Spectrometer (Thermo Fisher Scientific, Inc., USA). Samples were analyzed with three internal laboratory reference materials (ACELL $= 32.33 \pm 0.06‰$, JCELL-01 $= 17.64 \pm 0.09‰$, and SigmaCell $= 28.46 \pm 0.07‰$) calibrated against International Atomic Energy Agency (IAEA) benzoic acid reference materials: IAEA 601 ($23.24 \pm 0.19‰$) and IAEA 602 ($71.28 \pm 0.36‰$). A quality assurance sample (JCELL 02, $\delta^{18}O = 20.44 \pm 0.10‰$) was analyzed within each batch and analyzed as an unknown. The $\delta^{18}O_{cell}$ values had an analytical error of $\pm0.3‰$ and $\pm 0.1‰$ for the fossil and modern samples, respectively. The $\delta^{18}O_{cell}$ values are reported in units of per mil (‰) relative to the VSMOW standard.

3. Results

We recovered α–cellulose from 67% of the fossil wood samples (43 out of 64 samples); the remaining 21 samples (33%) contained no recoverable α–cellulose, and are not discussed further. The $\delta^{18}O_{cell}$ value of the 43 fossils ranged from 21.0 to 24.1‰ with a mean ($\pm 1\sigma$) = 22.4 $\pm 0.7‰$ (Table 1). The measured variance in the $\delta^{18}O_{cell}$ values across the 43 fossil specimens was small (0.5‰), consistent with a common water source and common environment during growth (Csank et al., 2013; Sternberg et al., 2007). Because the $\delta^{18}O$ value of seawater during the late Oligocene was lower than today (Westerhold et al., 2020), we added 2.5‰ to the fossil values to allow for an unbiased comparison with modern $\delta^{18}O_{cell}$ values. The $\delta^{18}O_{cell}$ value of the modern samples averaged 27.4 $\pm 1.0‰$ ($n = 22$) (Table 2), which was similar to the most recent 50 years of $\delta^{18}O_{cell}$ values measured independently on *Pinus massoniana* and *Picea schrenkiana* trees growing in monsoon regions of southern China (Shi et al., 2020; Xu et al., 2013) (Two-sample *t*-test, $t = 0.6$, $p = 0.53$). The different sampling resolution of the modern (annual) and fossil (bulk wood) samples do not allow for comparison of variance between the late Oligocene and present-day; however, the $\delta^{18}O_{cell}$ values of the modern samples is significantly higher than both the raw (22.4 $\pm 0.7‰$) and seawater-corrected (24.9 $\pm 0.7‰$) fossil $\delta^{18}O_{cell}$ values (two-sample *t*-tests, $t = 20.8$ and 10.3, respectively; $p < 0.0001$ for each). We note that all further analysis and discussion of the fossil $\delta^{18}O_{cell}$ data use the seawater corrected values.

4. Discussion

When examining our results within the context of published $\delta^{18}O_{cell}$ values, we find that all our measured $\delta^{18}O_{cell}$ values (both fossil and modern) were within the range of $\delta^{18}O_{cell}$ values reported for trees

Table 1
Measured $\delta^{18}O_{cell}$ values of late Oligocene fossil wood.

Sample ID	$\delta^{18}O_{cell}$ (‰, VSMOW)[a]	Sample ID	$\delta^{18}O_{cell}$ (‰, VSMOW)[a]
18,060–10	23.0	18,060–66	23.2
18,060-12A	22.5	18,060–70	23.0
18,060–13	22.1	18,060–71	22.0
18,060-15B	23.5	18,060–72	22.6
18,060–16	22.9	18,060–73	22.9
18,060–18	22.3	18,060–76	22.9
18,060–19	23.3	18,060–77	22.5
18,060–31	22.9	18,060–78	21.0
18,060–33	22.0	18,060–84	21.4
18,060–34	22.2	18,060–85	22.9
18,060–37	21.3	18,060–86	24.1
18,060–40	21.1	18,060–88	22.3
18,060–47	22.3	18,060–91	22.6
18,060–48	22.5	18,060–104	22.6
18,060–50	22.5	18,060–109	23.1
18,060–51	22.3	18,060–110	22.5
18,060–52	21.5	18,060–111	21.3
18,060–53	22.0	18,060–114	22.4
18,060–60	23.1	18,060–117	22.6
18,060–61	22.7	18,060–124	21.4
18,060–64	21.4	18,060–126	22.0
18,060–65	22.4	Average $\pm 1\sigma$	22.4 ± 0.5

[a] Data reported here are raw $\delta^{18}O_{cell}$ values, prior to any correction for changes in $\delta^{18}O$ of seawater. For comparison with modern values, we added 2.5‰ to these values to account for the lower $\delta^{18}O$ value of seawater during the late Oligocene than today, as inferred from $\delta^{18}O$ measurements of benthic foraminifera (Westerhold et al., 2020).

growing across the planet today ($\delta^{18}O_{cell} = 14$ to 34‰; Fig. 3). The $\delta^{18}O_{cell}$ values of the modern samples are similar to other records in southern China (Cai et al., 2018; Shi et al., 2020; Xu et al., 2013). However, our measured fossil $\delta^{18}O_{cell}$ values are lower than $\delta^{18}O_{cell}$ values from the modern trees in the Nanning Basin, and are more similar to values reported for trees growing at high elevation sites (3500 m) in Nepal (Xu et al., 2018); high latitude, cold sites near Lake Baikal in central Russia (Tartakovsky et al., 2012) and arctic Siberia (Holzkämper et al., 2008); and areas that receive higher summer rainfall amounts than southern China (e.g., Bangladesh, Islam et al., 2021). Nevertheless, the paleolatitude (Wu et al., 2017) and paleogeography (Quan et al., 2016) of Nanning Basin during the late Oligocene are incompatible with very low MAT and/or high elevation, suggesting the low $\delta^{18}O_{cell}$ values measured in our fossil wood samples are unlikely caused by these factors. This is also supported by similar $\delta^{18}O_{cell}$ values reported for

Table 2
Measured $\delta^{18}O_{cell}$ values for two modern tree cores (QXS21A and QXS24A).

Year	$\delta^{18}O_{cell}$ (‰, VSMOW)	
	QXS21A	QXS24A
1990	28.1	28.1
1991	29.1	27.9
1992	28.4	29.0
1993	28.5	28.0
1994	25.9	26.7
1995	26.5	26.7
1996	26.9	25.9
1997	26.4	25.7
1998	27.3	27.4
1999	26.4	27.4
2000	27.4	28.2
Average ± 1σ	27.4 ± 1.0	27.4 ± 1.0

Oligocene age wood fossils from interior Siberia (Fig. 3), which further preclude temperature (Richter et al., 2008b), vapor transport distance (Jahren and Sternberg, 2002), or continentality (i.e., distance from coast) (Rozanski et al., 1993) as viable explanations for the low $\delta^{18}O_{cell}$ values measured in the fossil wood from Nanning Basin. Intriguingly, similarly low $\delta^{18}O_{cell}$ values to our fossil wood have also been measured in modern wood growing within monsoon climates of east and south Asia that see greater precipitation amounts than present–day Nanning Basin (Islam et al., 2021; Schollaen et al., 2014; Zhu et al., 2012). For example, Zhu et al. (2012) reported $\delta^{18}O_{cell}$ values of 22.3 to 25.9‰ (mean ± 1σ = 24.1 ± 0.78‰) for *Pinus merkusii* growing in southern Cambodia and Islam et al. (2021) reported $\delta^{18}O_{cell}$ values of 24.2 to 27.2‰ for *Chukrasia tabularis* (25.6 ± 0.8‰) and *Lagerstroemia speciosa* (25.9 ± 0.5‰) growing in Bangladesh; both of these studies reported data from sites with greater wet-season precipitation than our study site in Nanning.

We therefore interpret our low $\delta^{18}O_{cell}$ values in terms of the amount effect, consistent with interpretations made at other low-elevation tropical and sub-tropical sites (Schollaen et al., 2014; Shi et al., 2020; Zhu et al., 2012), in which intense monsoon precipitation becomes depleted in ^{18}O in summer months (Araguás-Araguás et al., 1998; Dansgaard, 1964). We achieve this by first demonstrating the utility of these relationships for quantifying growing season precipitation in monsoon climates using our modern $\delta^{18}O_{cell}$ values, and then applying these relationships towards inferring wet-season rainfall during the late Oligocene using our fossil $\delta^{18}O_{cell}$ dataset.

4.1. Quantifying monsoon precipitation from $\delta^{18}O_{cell}$

In order to quantify monsoon rainfall from $\delta^{18}O_{cell}$, we first demonstrate the ability for $\delta^{18}O_{cell}$ to accurately record the $\delta^{18}O_{MW}$ value of monsoon rainfall in present-day Nanning. We did this by calculating $\delta^{18}O_{MW}$ from $\delta^{18}O_{cell}$ using the following relationship developed by Sternberg et al. (2007) from both needle leaf and broadleaf tree species growing across a wide climate gradient:

$$\delta^{18}O_{cell} = 0.60 \times \delta^{18}O_{MW} + 31.9 \qquad (1)$$

This relationship excluded samples from Arizona, USA (after Sternberg et al., 2007) because they grew under exceptionally low relative humidity (26%) that is known to affect $\delta^{18}O_{cell}$, and contrasts with the consistently high relative humidity of Nanning Basin today (80%) (Fig. 2). We note, however, that given the strong relationship between $\delta^{18}O_{cell}$ and $\delta^{18}O_{MW}$ and large sample size of this dataset ($n = 34$), the slope (m) and intercept (b) do not change substantially if the data from Arizona are included (m = 0.61, b = 32.4‰, Sternberg et al. (2007)).

Using Eq. (1) and the $\delta^{18}O_{cell}$ values measured here for the modern trees growing in Nanning, we calculate median $\delta^{18}O_{MW} = -7.5 \pm 1.7$‰ ($n = 22$). These values are consistent with predicted $\delta^{18}O_{MW}$ values for summer monsoon precipitation at this site, which today range from -6.5 to -8.0‰ (Fig. 2), and demonstrate the utility of Eq. (1) for estimating monsoon $\delta^{18}O_{MW}$ values using $\delta^{18}O_{cell}$.

Next, we calculated average monthly monsoon precipitation using the following relationship developed by Xie et al. (2011) for nearby Guangzhou, China:

$$P_{month} = -30.4 \times \delta^{18}O_{MW} - 0.5 \qquad (2)$$

where P_{month} is mean monthly precipitation, and $\delta^{18}O_{MW}$ is calculated using Eq. (1). Using our annual $\delta^{18}O_{cell}$ values from each tree core and Eqs. (1) and (2), we calculate mean (±1σ) P_{month} in Nanning today of 230 ± 51 mm (range = 141–314 mm). These values are consistent with average monthly rainfall amount during the wettest four months of each calendar year represented by our $\delta^{18}O_{cell}$ dataset, i.e., "P_{wet}" (1990–2000: P_{wet} = 216 ± 46 mm, range = 158–317 mm) (Fig. 4). This result highlights the importance of rainfall in the wettest months on tree growth in this subtropical monsoon climate, and suggests $\delta^{18}O_{cell}$ values as an accurate proxy for monsoon precipitation in the region.

4.2. Quantifying monsoon precipitation during the late Oligocene

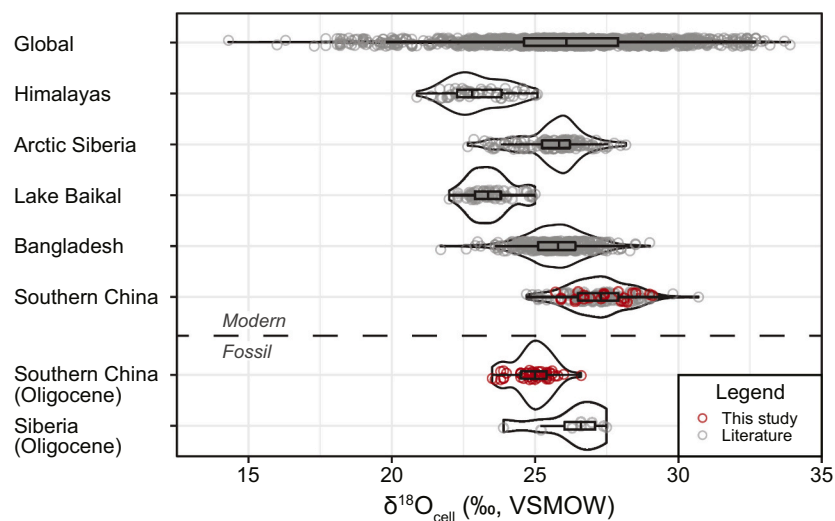Applying Eqs. (1) and (2) to our fossil wood data allows for

Fig. 3. Violin plots with $\delta^{18}O_{cell}$ data points, box plots, and kernel densities for modern and fossil samples. Late Oligocene values for Siberia and southern China have both been corrected by +2.5‰ to account for changes in seawater composition. Global data include compilations by Sternberg et al. (2007) and Richter et al. (2008b), with updated sites including a high elevation site in the Himalayas (Xu et al., 2018), high latitude site in acrtic Siberia (Holzkämper et al., 2008), inland/high latitude site in Lake Baikal (cetral Russia; Tartakovsky et al., 2012), and Bangladesh (Islam et al., 2021). Fossil data from Siberia are from Richter et al. (2008a). Box plots show the first through third quartiles with whiskers extending a distance of the interquartile range on either side of the box. All new modern data sets were trimmed to the most recent 50 years for each $\delta^{18}O_{cell}$ series to prevent overweighting individual sites. Data were available as supplementary materials from the primary publications. Data used in this figure are available in the supplementary materials (Table S1).
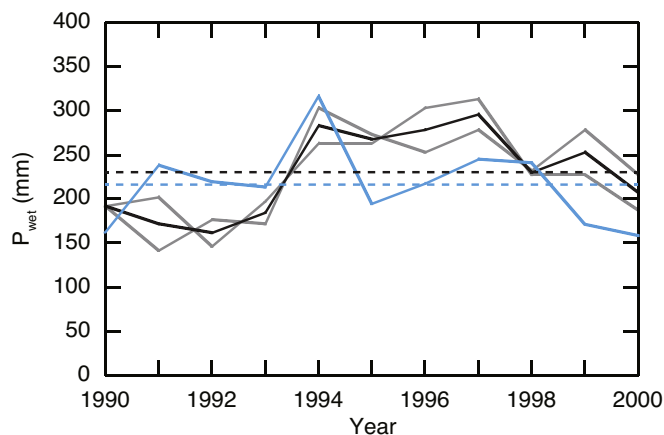
Fig. 4. Measured values for P_{wet} (blue) determined using monthly precipitation data from the Nanning weather station compared with reconstructed values for P_{wet} calculated using $\delta^{18}O_{cell}$ measured for each annual growth ring (Table 1) and Eqs. (1) and (2) (gray lines = individual cores QXS21A and QXS24A; black line = average of the two cores). Note the two-fold range of P_{wet} values (158 to 317 mm) represented by the 11 year record. We find no significant difference between the average actual and reconstructed P_{wet} values (*t*-test, $t = -0.67$, $p = 0.51$) (dashed lines), suggesting that the measured $\delta^{18}O_{cell}$ values are reflecting average rainfall in only the wettest months of the calendar year. (For interpretation of the references to colour in this figure legend, the reader is referred to the web version of this article.)

estimation of monsoon precipitation during the late Oligocene. We note that this approach can be affected by changes in the $\delta^{18}O$ value of source water and potential changes in $\delta^{18}O_{MW}$ gradients through time (Fricke and O'Neil, 1999). If we assume a similar amount effect in the late Oligocene as today, we can use our seawater-adjusted fossil $\delta^{18}O_{cell}$ values to calculate average $P_{wet} = 349 \pm 35$ mm ($n = 43$), which suggests late Oligocene rainfall was approximately 60% greater than present-day ($P_{wet} = 220 \pm 46$ mm, 1951 to 2012) (note, without the correction, $P_{wet} = 476$ mm, or 2.2× present-day, which is untenably large). Today, similar monthly precipitation amounts are found at coastal sites only 400 km to the southeast of Nanning (e.g., $P_{wet} = 354$ mm at Yangjiang, China) as well as large portions of north central Vietnam and central Laos ($P_{wet} = 339$ mm, range = 315 to 383 mm) and central Bangladesh ($P_{wet} = 348$ mm, range = 314 to 384 mm). We note that our significantly lower $\delta^{18}O_{cell}$ values in the late Oligocene compared with today cannot be reconciled without an increase in rainfall compared to present, even if the specific relationship represented by Eq. (2) differed in the past (e.g., steeper or shallower slope). Although the exact amount of this increase is here calculated as 60%, larger and smaller increases cannot be ruled out without knowing $\delta^{18}O_{MW}/P_{wet}$ spatial patterns in the late Oligocene.

Recent efforts have aimed to improve our understanding of spatial patterns in precipitation during the late Oligocene (Utescher et al., 2021). Plant macrofossil data indicate less wet-season precipitation in northern China during this time (Li et al., 2018), in contrast with the greater wet-season rainfall we calculate here for southern China. These regional differences are consistent with observations and models indicating diminished rainfall in northern China (Li et al., 2017) and increased rainfall to the south (Bryan et al., 2019; Sooraj et al., 2015) in response to modern global warming, and lend support to our interpretation of high rainfall inferred by the low $\delta^{18}O_{cell}$ values. The increased average wet season rainfall calculated here for the late Oligocene further supports hypotheses that warmer temperatures in the future will increase the amount of precipitable water thereby intensifying rainfall in southern China (Takahashi et al., 2020). This interpretation is supported by multiple models that indicate a 50% to 100% increase in extreme precipitation frequency in southern China and southeast Asia in response to warming of only 1.5 to 2 °C (Chevuturi et al., 2018).

The Oligocene paleoflora at Nanning has previously been interpretated to reflect tropical, monsoonal climate conditions similar to areas that receive higher summer rainfall than modern Nanning (e.g., Thailand and eastern India; Huang et al., 2018; Ying et al., 2018). The results of the current study and these independent lines of evidence suggest that the East Asian monsoon was at least as strong as modern conditions—with likely higher summer rainfall levels—during the late Oligocene, and indicates that the East Asian monsoon may strengthen as CO_2 levels and global temperatures approach those of the Oligocene (Tierney et al., 2020).

5. Conclusions

We show that $\delta^{18}O_{cell}$ values can be used to provide information on summer rainfall within monsoon regions. We find that $\delta^{18}O_{cell}$ values were 5‰ lower during the late Oligocene than today, half of which is attributed to lower $\delta^{18}O$ values of seawater and half to changes in climate. Comparison to Oligocene $\delta^{18}O_{cell}$ data from Siberia confirm the low $\delta^{18}O_{cell}$ values cannot be reconciled by lower temperatures because it is unlikely both sites experienced the same temperatures. Agreement between $\delta^{18}O_{cell}$ and rainfall in modern monsoon regions supports our interpretation of low fossil $\delta^{18}O_{cell}$ values inferring elevated rainfall during the late Oligocene. Using modern relationships, we calculate a 59% increase in monsoon rainfall during the late Oligocene compared to present (349 mm/month versus 220 mm/month). Such heavy rainfall in a single month is not unprecedented in Nanning at present: from 1951 to 2012, nearly 10% of the monsoon months (May through August) have experienced at least 349 mm of rainfall; however, no single year has averaged at least 349 mm across four months (i.e., $P_{wet} \geq 349$ mm, the late Oligocene average value). This result is consistent with fundamentally higher monsoon rainfall in the late Oligocene than today and indicates potential for greater monsoon rainfall in a warmer climate. We therefore conclude that continued global warming beyond 2 °C may lead to enhancement of wet-season rainfall in southern regions of the East Asian monsoon.

Declaration of Competing Interest

The authors declare that they have no known competing financial interests or personal relationships that could have appeared to influence the work reported in this paper.

Appendix A. Supplementary data

Supplementary data to this article can be found online at https://doi.org/10.1016/j.palaeo.2021.110556.

References

Araguás-Araguás, L., Froehlich, K., Rozanski, K., 1998. Stable isotope composition of precipitation over Southeast Asia. JGR 103, 28721–28742.
Bollasina, M.A., Ming, Y., Ramaswamy, V., 2011. Anthropogenic aerosols and the weakening of the South Asian summer monsoon. Sci 334, 502–505.
Bowen, G.J., 2008. Spatial analysis of the intra-annual variation of precipitation isotope ratios and its climatological corollaries. J. Geophys. Res. 113, D05113.

Bowen, G.J., Wassenaar, L.I., Hobson, K.A., 2005. Global application of stable hydrogen and oxygen isotopes to wildlife forensics. Oecologia 143, 337–348.

Brendel, O., Iannetta, P.P.M., Stewart, D., 2000. A rapid and simple method to isolate pure α-cellulose. Phytochem. Anal. 11, 7–10.

Brienen, R.J.W., Helle, G., Pons, T.L., Guyot, J.-L., Gloor, M., 2012. Oxygen isotopes in tree rings are a good proxy for Amazon precipitation and El Niño-Southern Oscillation variability. Proc. Natl. Acad. Sci. 109, 16957–16962.

Bryan, S.P., Hughen, K.A., Karnauskas, K.B., Farrar, J.T., 2019. Two hundred fifty years of reconstructed South Asian summer monsoon intensity and decadal-scale variability. Geophys. Res. Lett. 46, 3927–3935.

Büntgen, U., Kolář, T., Rybníček, M., Koňasová, E., Trnka, M., Ač, A., Krusic, P.J., Esper, J., Treydte, K., Reinig, F., Kirdyanov, A., Herzig, F., Urban, O., 2020. No age trends in oak stable isotopes. Paleoceanogr. Paleoclimatol. 35 e2019PA003831.

Cai, Q., Liu, Y., Duan, B., Li, Q., Sun, C., Wang, L., 2018. Tree-ring δ18O, a tool to crack the paleo-hydroclimatic code in subtropical China. Quat. Int. 487, 3–11.

Cheng, H., Edwards, R.L., Sinha, A., Spötl, C., Yi, L., Chen, S., Kelly, M., Kathayat, G., Wang, X., Li, X., Kong, X., Wang, Y., Ning, Y., Zhang, H., 2016. The Asian monsoon over the past 640,000 years and ice age terminations. Nature 534, 640–646.

Chevuturi, A., Klingaman, N.P., Turner, A.G., Hannah, S., 2018. Projected changes in the Asian-Australian Monsoon Region in 1.5°C and 2.0°C Global-warming scenarios. Earth's Future 6, 339–358.

China Meteorological Data Service Center, 2018. Station No. 59431, Nanning City.

Cosford, J., Qing, H., Eglington, B., Mattey, D., Yuan, D., Zhang, M., Cheng, H., 2008. East Asian monsoon variability since the Mid-Holocene recorded in a high-resolution, absolute-dated aragonite speleothem from eastern China. E&PSL 275, 296–307.

Csank, A.Z., Fortier, D., Leavitt, S.W., 2013. Annually resolved temperature reconstructions from a late Pliocene–early Pleistocene polar forest on Bylot Island, Canada. Palaeogeogr. Palaeoclimatol. Palaeoecol. 369, 313–322.

Dansgaard, W., 1964. Stable isotopes in precipitation. Tell 16, 436–468.

Dayem, K.E., Molnar, P., Battisti, D.S., Roe, G.H., 2010. Lessons learned from oxygen isotopes in modern precipitation applied to interpretation of speleothem records of paleoclimate from eastern Asia. E&PSL 295, 219–230.

Dong, B., Wilcox, L.J., Highwood, E.J., Sutton, R.T., 2019. Impacts of recent decadal changes in Asian aerosols on the East Asian summer monsoon: roles of aerosol–radiation and aerosol–cloud interactions. ClDy 53, 3235–3256.

Duffy, J.E., McCarroll, D., Loader, N.J., Young, G.H.F., Davies, D., Miles, D., Bronk Ramsey, C., 2019. Absence of age-related trends in stable oxygen isotope ratios from oak tree ring series. GBioC 33, 841–848.

Fang, X., Dupont-Nivet, G., Wang, C., Song, C., Meng, Q., Zhang, W., Nie, J., Zhang, T., Mao, Z., Chen, Y., 2020. Revised chronology of Central Tibet uplift (Lunpola Basin). Sci. Adv. 6 eaba7298.

Farnsworth, A., Lunt, D.J., Robinson, S.A., Valdes, P.J., Roberts, W.H.G., Clift, P.D., Markwick, P., Su, T., Wrobel, N., Bragg, F., Kelland, S.-J., Pancost, R.D., 2019. Past East Asian monsoon evolution controlled by paleogeography, not CO2. Sci. Adv. 5 eaax1697.

Fricke, H.C., O'Neil, J.R., 1999. The correlation between 18O/16O ratios of meteoric water and surface temperature: its use in investigating terrestrial climate change over geologic time. E&PSL 170, 181–196.

Gee, C.T., Sander, P.M., Petzelberger, B.E.M., 2003. A Miocene Rodent Nut Cache in coastal Dunes of the Lower Rhine Embayment, Germany, 46, pp. 1133–1149.

Gonfiantini, R., Roche, M.-A., Olivry, J.-C., Fontes, J.-C., Zuppi, G.M., 2001. The altitude effect on the isotopic composition of tropical rains. ChGeo 181, 147–167.

Hao, Y.-R., Peng, S.-L., Mo, J.-M., Liu, X.-W., Chen, Z.-Q., Zhou, K., Wu, J.-R., 2006. Roots of pioneer trees in the lower sub-tropical area of Dinghushan, Guangdong, China. J Zhejiang Univ Sci B 7, 377–385.

Holzkämper, S., Kuhry, P., Kultti, S., Gunnarson, B., Sonninen, E., 2008. Stable isotopes in tree rings as proxies for winter precipitation changes in the Russian Arctic over the past 150 years. Geochronometria 32, 37–46.

Huang, L., Jin, J., Quan, C., Oskolski, A.A., 2018. Mummified fossil woods of Fagaceae from the upper Oligocene of Guangxi, South China. JAESc 152, 39–51.

Huang, R., Zhu, H., Liang, E., Grießinger, J., Dawadi, B., Bräuning, A., 2019a. High-elevation shrub-ring δ18O on the northern slope of the Central Himalayas records summer (May–July) temperatures. Palaeogeogr. Palaeoclimatol. Palaeoecol. 524, 230–239.

Huang, R., Zhu, H., Liang, E., Grießinger, J., Wernicke, J., Yu, W., Hochreuther, P., Risi, C., Zeng, Y., Fremme, A., Sodemann, H., Bräuning, A., 2019b. Temperature signals in tree-ring oxygen isotope series from the northern slope of the Himalaya. E&PSL 506, 455–465.

Islam, M., Rahman, M., Gebrekirstos, A., Bräuning, A., 2021. Tree-ring δ18O climate signals vary among tree functional types in South Asian tropical moist forests. Sci. Total Environ. 756, 143939.

Jahren, A.H., Sternberg, L.S.L., 2002. Eocene meridional weather patterns reflected in the oxygen isotopes of Arctic fossil wood. GSA Today 12, 4–9.

Jahren, A.H., Sternberg, L.S.L., 2003. Humidity estimate for the middle Eocene Arctic rain forest. Geology 31, 463–466.

Jahren, A.H., Sternberg, L.S.L., 2008. Annual patterns within tree rings of the Arctic middle Eocene (ca. 45 Ma): isotopic signatures of precipitation, relative humidity, and deciduousness. Geology 36, 99–102.

Kim, M.J., Yeh, S.-W., Park, R.J., 2016. Effects of sulfate aerosol forcing on East Asian summer monsoon for 1985–2010. Geophys. Res. Lett. 43, 1364–1372.

Knorre, A.A., Siegwolf, R.T.W., Saurer, M., Sidorova, O.V., Vaganov, E.A., Kirdyanov, A.V., 2010. Twentieth century trends in tree ring stable isotopes (δ13C and δ18O) of *Larix sibirica* under dry conditions in the forest steppe in Siberia. J. Geophys. Res. Biogeosci. 115 https://doi.org/10.1029/2009jg000930.

Li, X., Cheng, H., Tan, L., Ban, F., Sinha, A., Duan, W., Li, H., Zhang, H., Ning, Y., Kathayat, G., Edwards, R.L., 2017. The East Asian summer monsoon variability over the last 145 years inferred from the Shihua Cave record, North China. Sci. Rep. 7, 7078.

Li, S., Xing, Y., Valdes, P.J., Huang, Y., Su, T., Farnsworth, A., Lunt, D.J., Tang, H., Kennedy, A.T., Zhou, Z., 2018. Oligocene climate signals and forcings in Eurasia revealed by plant macrofossil and modelling results. Gondwana Res. 61, 115–127.

Licht, A., van Cappelle, M., Abels, H.A., Ladant, J.B., Trabucho-Alexandre, J., France-Lanord, C., Donnadieu, Y., Vandenberghe, J., Rigaudier, T., Lecuyer, C., Terry Jr., D., Adriaens, R., Boura, A., Guo, Z., Soe, A.N., Quade, J., Dupont-Nivet, G., Jaeger, J.J., 2014. Asian monsoons in a late Eocene greenhouse world. Nature 513, 501–506.

Liu, G., Li, X., Chiang, H.-W., Cheng, H., Yuan, S., Chawchai, S., He, S., Lu, Y., Aung, L.T., Maung, P.M., Tun, W.N., Oo, K.M., Wang, X., 2020. On the glacial-interglacial variability of the Asian monsoon in speleothem δ18O records. Sci. Adv. 6 eaay8189.

Loader, N.J., McCarroll, D., Gagen, M., Robertson, I., Jalkanen, R., 2007. Extracting climatic information from stable isotopes in tree rings. In: Dawson, T.E., Siegwolf, R.T.W. (Eds.), Stable Isotopes as Indicators of Ecological Change. Elsevier, pp. 27–48.

Loader, N.J., Helle, G., Los, S.O., Lehmkuhl, F., Schleser, G.H., 2010. Twentieth-century summer temperature variability in the southern Altai Mountains: a carbon and oxygen isotope study of tree-rings. Holocene 20, 1149–1156.

McCarroll, D., Loader, N.J., 2004. Stable isotopes in tree rings. QSRv 23, 771–801.

Mu, J., Wang, Z., 2021. Responses of the East Asian summer monsoon to aerosol forcing in CMIP5 models: the role of upper-tropospheric temperature change. IJCli 41, 1555–1570.

Olson, E.J., Dodd, J.P., Rivera, M.A., 2020. *Prosopis* sp. tree-ring oxygen and carbon isotope record of regional-scale hydroclimate variability during the last 9500 years in the Atacama Desert. Palaeogeogr. Palaeoecol. 538, 109408.

Poussart, P.F., Evans, M.N., Schrag, D.P., 2004. Resolving seasonality in tropical trees: multi-decade, high-resolution oxygen and carbon isotope records from Indonesia and Thailand. E&PSL 218, 301–316.

Quan, C., Qiongyao, F., Shi, G., Liu, C.Y., Li, L., Liu, X., Jin, J., 2016. First Oligocene mummified plant Lagerstätte at the low latitudes of East Asia. Sci. China Earth Sci. 59.

Ramage, C.S., 1971. Monsoon Meteorology. Academic Press, Inc., New York.

Richter, S.L., Johnson, A.H., Dranoff, M.M., LePage, B.A., Williams, C.J., 2008a. Oxygen isotope ratios in fossil wood cellulose: isotopic composition of Eocene- to Holocene-aged cellulose. Geochim. Cosmochim. Acta 72, 2744–2753.

Richter, S.L., Johnson, A.H., Dranoff, M.M., Taylor, K.D., 2008b. Continental-scale patterns in modern wood cellulose δ18O: implications for interpreting paleo-wood cellulose δ18O. Geochim. Cosmochim. Acta 72, 2735–2743.

Rinne, K.T., Loader, N.J., Switsur, V.R., Waterhouse, J.S., 2013. 400-year May–August precipitation reconstruction for Southern England using oxygen isotopes in tree rings. QSRv 60, 13–25.

Rozanski, K., Araguás-Araguás, L., Gonfiantini, R., 1993. Isotopic patterns in modern global precipitation. In: Swart, P.K., Lohmann, K.C., MacKenzie, J., Savin, S. (Eds.), Climate Change in Continental Records. American Geophysical Union, Washington, DC, pp. 1–37.

Sakashita, W., Yokoyama, Y., Miyahara, H., Yamaguchi, Y.T., Aze, T., Obrochta, S.P., Nakatsuka, T., 2016. Relationship between early summer precipitation in Japan and the El Niño-Southern and Pacific Decadal Oscillations over the past 400 years. Quat. Int. 397, 300–306.

Saurer, M., Cherubini, P., Reynolds-Henne, C.E., Treydte, K.S., Anderson, W.T., Siegwolf, R.T.W., 2008. An investigation of the common signal in tree ring stable isotope chronologies at temperate sites. J. Geophys. Res. 113, G04035.

Saurer, M., Kirdyanov, A.V., Prokushkin, A.S., Rinne, K.T., Siegwolf, R.T.W., 2016. The impact of an inverse climate–isotope relationship in soil water on the oxygen-isotope composition of Larix gmelinii in Siberia. New Phytol. 209, 955–964.

Schollaen, K., Heinrich, I., Helle, G., 2014. UV-laser-based microscopic dissection of tree rings – a novel sampling tool for δ13C and δ18O studies. New Phytol. 201, 1045–1055.

Schubert, B.A., Jahren, A.H., 2015. Seasonal temperature and precipitation recorded in the intra-annual oxygen isotope pattern of meteoric water and tree-ring cellulose. QSRv 125, 1–14.

Shi, S., Shi, J., Xu, C., Leavitt, S.W., Wright, W.E., Cai, Z., Zhang, H., Sun, X., Zhao, Y., Ma, X., Zhang, W., Lu, H., 2020. Tree-ring δ18O from Southeast China reveals monsoon precipitation and ENSO variability. Palaeogeogr. Palaeoclimatol. Palaeoecol. 558, 109954.

Sooraj, K.P., Terray, P., Mujumdar, M., 2015. Global warming and the weakening of the Asian summer monsoon circulation: assessments from the CMIP5 models. ClDy 45, 233–252.

Sternberg, L.D.L., Pinzon, M.C., Vendramini, P.F., Anderson, W.T., Jahren, A.H., Beuning, K., 2007. Oxygen isotope ratios of cellulose-derived phenylglucosazone: an improved paleoclimate indicator of environmental water and relative humidity. Geochim. Cosmochim. Acta 71, 2463–2473.

Su, T., Farnsworth, A., Spicer, R.A., Huang, J., Wu, F.-X., Liu, J., Li, S.-F., Xing, Y.-W., Huang, Y.-J., Deng, W.-Y.-D., Tang, H., Xu, C.-L., Zhao, F., Srivastava, G., Valdes, P.J., Deng, T., Zhou, Z.-K., 2019. No high Tibetan Plateau until the Neogene. Sci. Adv. 5 eaav2189.

Takahashi, H.G., Kamizawa, N., Nasuno, T., Yamada, Y., Kodama, C., Sugimoto, S., Satoh, M., 2020. Response of the Asian Summer Monsoon precipitation to global warming in a high-resolution global nonhydrostatic model. J. Clim. 33, 8147–8164.

Tartakovsky, V.A., Voronin, V.I., Markelova, A.N., 2012. External forcing factor reflected in the common signals of δ18O-tree-ring series of *Larix sibirica* Ledeb. in the Lake Baikal region. Dendrochronologia 30, 199–208.

Tierney, J.E., Poulsen, C.J., Montañez, I.P., Bhattacharya, T., Feng, R., Ford, H.L., Hönisch, B., Inglis, G.N., Petersen, S.V., Sagoo, N., Tabor, C.R., Thirumalai, K.,

Zhu, J., Burls, N.J., Foster, G.L., Goddéris, Y., Huber, B.T., Ivany, L.C., Kirtland Turner, S., Lunt, D.J., McElwain, J.C., Mills, B.J.W., Otto-Bliesner, B.L., Ridgwell, A., Zhang, Y.G., 2020. Past climates inform our future. Sci 370 eaay3701.

Treydte, K.S., Schleser, G.H., Helle, G., Frank, D.C., Winiger, M., Haug, G.H., Esper, J., 2006. The twentieth century was the wettest period in northern Pakistan over the past millennium. Nature 440, 1179–1182.

Utescher, T., Erdei, B., François, L., Henrot, A.-J., Mosbrugger, V., Popova, S., 2021. Oligocene vegetation of Europe and western Asia—Diversity change and continental patterns reflected by plant functional types. GeolJ 56, 628–649.

Vornlocher, J.R., Lukens, W.E., Schubert, B.A., Quan, C., 2021. Late Oligocene precipitation seasonality in East Asia based on $\delta^{13}C$ profiles in fossil wood. Paleoceanogr. Paleoclimatol. 36 e2021PA004229.

Wang, B., Ding, Q.H., 2008. Global monsoon: dominant mode of annual variation in the tropics. DyAtO 44, 165–183.

Wang, B., LinHo, 2002. Rainy season of the Asian-Pacific summer monsoon. J. Clim. 15, 386–398.

Waterhouse, J.S., Switsur, V.R., Barker, A.C., Carter, A.H.C., Robertson, I., 2002. Oxygen and hydrogen isotope ratios in tree rings: how well do models predict observed values? E&PSL 201, 421–430.

Westerhold, T., Marwan, N., Drury, A.J., Liebrand, D., Agnini, C., Anagnostou, E., Barnet, J.S.K., Bohaty, S.M., De Vleeschouwer, D., Florindo, F., Frederichs, T., Hodell, D.A., Holbourn, A.E., Kroon, D., Lauretano, V., Littler, K., Lourens, L.J., Lyle, M., Pälike, H., Röhl, U., Tian, J., Wilkens, R.H., Wilson, P.A., Zachos, J.C., 2020. An astronomically dated record of Earth's climate and its predictability over the last 66 million years. Sci 369, 1383–1387.

Wolfe, A.P., Csank, A.Z., Reyes, A.V., McKellar, R.C., Tappert, R., Muehlenbachs, K., 2012. Pristine Early Eocene wood buried deeply in kimberlite from northern Canada. PLoS One 7, e45537.

Wu, L., Kravchinsky, V.A., Potter, D.K., 2017. Apparent polar wander paths of the major Chinese blocks since the Late Paleozoic: toward restoring the amalgamation history of East Eurasia. Earth-Sci. Rev. 171, 492–519.

Xie, L.H., Wei, G.J., Deng, W.F., Zhao, X.L., 2011. Daily $\delta^{18}O$ and δD of precipitations from 2007 to 2009 in Guangzhou, South China: implications for changes of moisture sources. JHyd 400, 477–489.

Xu, C., Zheng, H., Nakatsuka, T., Sano, M., 2013. Oxygen isotope signatures preserved in tree ring cellulose as a proxy for April–September precipitation in Fujian, the subtropical region of Southeast China. J. Geophys. Res.-Atmos. 118, 12,805–812,815.

Xu, C., Zheng, H., Nakatsuka, T., Sano, M., Li, Z., Ge, J., 2016. Inter- and intra-annual tree-ring cellulose oxygen isotope variability in response to precipitation in Southeast China. Trees 30, 785–794.

Xu, C., Sano, M., Dimri, A.P., Ramesh, R., Nakatsuka, T., Shi, F., Guo, Z., 2018. Decreasing Indian summer monsoon on the northern Indian sub-continent during the last 180 years: evidence from five tree-ring cellulose oxygen isotope chronologies. Clim. Past 14, 653–664.

Young, G.F., Loader, N., McCarroll, D., Bale, R., Demmler, J., Miles, D., Nayling, N., Rinne, K., Robertson, I., Watts, C., Whitney, M., 2015. Oxygen stable isotope ratios from British oak tree-rings provide a strong and consistent record of past changes in summer rainfall. ClDy 1–14.

Zhu, M.F., Stott, L., Buckley, B., Yoshimura, K., Ra, K., 2012. Indo-Pacific Warm Pool convection and ENSO since 1867 derived from Cambodian pine tree cellulose oxygen isotopes. J. Geophys. Res.-Atmos. 117.